PHYSICAL REVIEW B VOLUME 5, NUMBER 8 15 APRIL 1972

Lattice Thermal Conductivity of *p*-Type Mercury Telluride*

Charles R. Whitsett and Donald A. Nelson
McDonnell Douglas Research Laboratories, McDonnell Douglas Corporation,
St. Louis, Missouri 63166
(Received 25 August 1971)

The lattice thermal conductivity between 1.7 and 150 K of *p*-type mercury telluride is reported. For most of this temperature range the thermal-conductivity behavior is similar to that of other valence or ionic crystals, but at the lowest temperatures the thermal conductivity is limited, not by boundary scattering of phonons, but apparently by hole-phonon scattering. The Callaway phenomenological model is used to fit the data and to obtain the magnitudes of the normal-, umklapp-, and Rayleigh-scattering relaxation times. Although the hole concentrations of the samples ranged from 5.0×10^{16} to 4.4×10^{18} cm^{-3}, the magnitude of the inverse relaxation time for the scattering of phonons by holes did not vary significantly and was approximately $2.7q$ sec^{-1} for the phonon wave number q less than 6×10^{6} cm^{-1}. This behavior is attributed to the complex shape of the hole Fermi surface. As the hole concentration of HgTe increases, the maximum dimension of the hole Fermi surface increases relatively slowly because of the overlapping valence and conduction bands, and thus the range of wave numbers of phonons which can interact with holes is only weakly dependent upon the density of holes. Measurements of the thermoelectric power also are reported, and the same hole-phonon-scattering relaxation time required to explain the low-temperature thermal conductivity accounts for the phonon-drag contribution to the thermoelectric power.

I. INTRODUCTION

Mercury telluride (HgTe) is a semimetal which crystallizes in the cubic zinc-blende structure. It is similar to grey tin in that it has the same inverted band structure[1] with the conduction band degenerate with the valence band at the Brillouin zone center; it is different, however, in that the valence band slightly overlaps the conduction band in the $\langle 111\rangle$ and $\langle 110\rangle$ directions of k space.[2,3] This close similarity of the compound to the element makes it attractive for fundamental solid state physics studies. Additionally, HgTe has attracted a number of investigators because its mixtures with cadmium telluride (CdTe) are small-band-gap semiconductors which are used to fashion efficient, intrinsic, photoconductive detectors of far infrared radiation.[4]

This paper reports the lattice thermal conductivity of *p*-type HgTe over the temperature range 1.7–150 K. For most of this temperature range the thermal conductivity behavior is similar to that of other valence or ionic crystals, but at the lowest temperatures the thermal conductivity is very much lower than would be expected if scattering of phonons by the crystal boundaries were the limiting mechanism. A simple analysis shows that this depression of the thermal conductivity at low temperatures must be largely the result of hole-phonon scattering, and this conclusion is strengthened by the fact that the same hole-phonon-scattering relaxation time can be used to describe both the thermal conductivity and the phonon-drag contribution to the thermoelectric power.

The thermal conductivity below 60 K of *p*-type HgTe has not been previously reported. In 1958, Carlson[5] reported the thermal conductivity of a *p*-type HgTe sample which at low temperatures had a hole concentration of about 1.5×10^{18} cm^{-3}. He presented data for the temperature interval 60–300 K, over which phonon scattering occurs predominantly by umklapp processes. For the room-temperature thermal conductivity of HgTe, Carlson obtained the value 0.027 W cm^{-1} K^{-1}. Kolosov and Sharavskii[6] later obtained essentially the same result for a number of HgTe samples with hole concentrations between 3×10^{17} and 10^{19} cm^{-3}; their data were for temperatures between 90 and 430 K, and their average value for the total thermal conductivity of HgTe at 300 K was 0.026 W cm^{-1} K^{-1}. In a study of the thermal and electrical properties of the HgTe-CdTe system, Markert, Nieke, and Spiegler[7] included results for pure HgTe between 80 and 450 K; at room temperature they obtained 0.027 W cm^{-1} K^{-1} for the total thermal conductivity and, by subtracting calculated electronic and bipolar diffusion contributions, 0.024 W cm^{-1} K^{-1} for the lattice thermal conductivity. Muzhdaba *et al.*[8] measured the thermal conductivity between 4.2 and 200 K of an *n*-type HgTe crystal with an electron concentration of 3×10^{18} cm^{-3}, but they made no analysis of the data. Their chief interest was the deduction of the Lorenz number for the electronic thermal conductivity from the magnetic field dependence of the total thermal conductivity. They found that the Lorenz number decreased from L_0

at 4.2 K to 0.78 L_0 at 200 K, where L_0 is the Sommerfeld value of 2.44×10^{-8} W Ω K^{-2}.

II. EXPERIMENTAL PROCEDURE

The HgTe compound was prepared and single crystals were grown by methods similar to those previously described by the authors for HgSe[9] and by Lawson *et al.*[10] for HgTe. The elemental constituents, in stoichiometric proportions to form HgTe, were sealed within an evacuated, thick-walled, quartz capsule (12-mm i.d., 3-mm wall thickness) and then reacted in a rocking furnace at a temperature of about 750 °C for several hours. The resultant encapsulated ingot of compound was then situated in a horizontally-traveling, zone-melting furnace. The furnace, as it traveled, maintained the entire length of the stationary ingot at a temperature a few degrees below the 690 °C melting temperature, except for the molten zone which was maintained at a few degrees above the melting temperature and which was, typically, about 3 cm long. The ingot from which samples were cut for this investigation was subjected to two molten zone passages, the first to produce a uniform cross-section for the length of the ingot and the second to obtain single crystal formation. The recrystallized ingot was slowly cooled to room temperature. Two single-crystal samples for this study, HgTe 2 and HgTe 3, each $0.31\times0.31\times5.0$ cm initially, were cut from this ingot. Each crystal sample was mechanically polished, the final polish being obtained with 0.05-μm-diam-particle-size alumina abrasive.

The as-grown crystals of HgTe had hole concentrations of 1.17×10^{18} cm^{-3} at 4.2 K. (The procedure used for calculating the charge-carrier concentrations is described in the Appendix.) In general, HgTe annealed in vacuum at 200–250 °C becomes more p-type, and HgTe annealed in Hg vapor becomes less p-type and eventually n-type.[11,12] Excess hole concentrations probably are due either to interstitial Te or to Hg vacancies, or both. The annealing histories of the HgTe thermal-conductivity samples are summarized in Table I.

TABLE I. Thermal histories of the HgTe thermal-conductivity samples. As-grown samples were cooled slowly from the 690 °C melting temperature.

HgTe sample No.	Thermal history
2-1	As-grown
2-2	HgTe 2-1 subsequently annealed in Hg vapor at 250 °C for 100 h.
2-3	HgTe 2-2 subsequently annealed in vacuum at 225 °C for 72 h.
3-1	Annealed in He (3 Torr at 300 K) at 400 °C for 1 h, then rapidly quenched to 77 K.
3-2	HgTe 3-1 subsequently annealed in Hg vapor at 250 °C for 100 h.

The absolute, steady-state, longitudinal-heat-flow method was used to determine the thermal conductivity. With this method a temperature gradient dT/dx is established along the length of the sample by introducing a heat flow W at one end and extracting it at the other end. If no heat is lost through the sides of the sample, the thermal conductivity is

$$\kappa = \frac{W}{\mathfrak{A}}\left(\frac{dT}{dx}\right)^{-1} , \qquad (1)$$

where $\mathfrak{A}$ is the cross sectional area of the sample.

The apparatus used was similar to that described by Holland and Rubin,[13] and techniques described by Rhodes, Moeller, and Sauer[14] were closely followed. Carbon resistors, mounted on copper bars as described by Anderson, Reese, and Wheatley,[15] were used both for temperature and temperature-differential measurements below 7.5 K. Above 7.5 K, a copper-constantan thermocouple was used for measurement of absolute temperature, and manganin–gold-cobalt–manganin differential thermocouples were used for measurements of temperature gradients. The copper bars upon which were mounted the differential thermocouples as well as the carbon resistors were held against the side of a sample with phosphor-bronze spring clips.

Figure 1 depicts a cross section of the sample chamber, which is suspended from the top of a Dewar by a stainless-steel tube. In use, the entire sample chamber is immersed in liquid helium or other cryogen and is evacuated through the stainless-steel suspension tube. A heat leak thermally connects the sample mounting block to the base of the sample chamber. High-purity Pb was chosen as the heat-leak material because above 7 K its thermal conductivity decreases rapidly as the temperature increases, which obviates the use of a number of different cryogens or different sizes of heat leaks for different ranges of sample temperature. For our thermal conductivity probe, the heat leak was a strip of 99.999%-pure Pb, 0.15×0.25 cm^2 in cross section and 8.0 cm in length. With this heat leak a heat input of 30 mW raised the sample temperature to 4.5 K when the probe was immersed in liquid helium at 1.7 K, and sample-block temperatures up to 150 K were achievable. The upper temperature of the sample block was not limited by the Pb heat leak, but rather by the radiative transfer of heat from the sample block and radiation shield to the

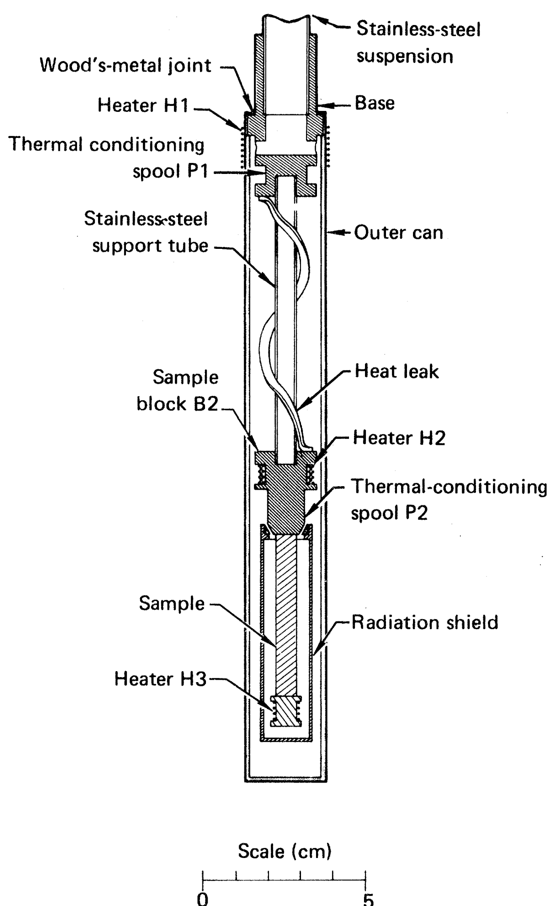

FIG. 1. Cross section of that portion of the thermal-conductivity apparatus which is immersed in liquid cryogen.

outer wall.

Thin copper plates were ultrasonically soldered with pure tin to each end of a HgTe thermal-conductivity sample. The copper end-plates were in turn soldered with Wood's metal to the sample block and sample heater. This technique eliminated sample fracture which is often caused by temperature cycling, and it provided satisfactorily low thermal-resistance paths between the components.

Radiation-loss corrections to the measured thermal conductivity were made, based upon calculations which were believed to be accurate to within a factor of two. The maximum possible error in the measurement of total thermal conductivity was estimated to be ± 4.5% at temperatues lower than 100 K, ± 5.5% at 125 K, and ± 9.0% at 155 K. The increase in the error with temperature is due primarily to the correspondingly increasing importance of radiation loss.

The low-field Hall coefficient as a function of temperature between 4.2 and 300 K is shown for each sample in Fig. 2, and the electrical conductivities are shown in Fig. 3. From these data the electron and hole concentrations were calculated by the method described in the Appendix, and the results at 4.2, 77, and 290 K are listed in Table II. The samples, except possibly HgTe 2-2, were p-type with hole concentrations at 4.2 K ranging from 5.0×10^{16} to 4.4×10^{18} holes/cm^3. As is explained in the Appendix, the electrical characteristics of HgTe 2-2 were anomalous and the actual nature of this sample could not be unambiguously determined.

III. LATTICE THERMAL CONDUCTIVITY

The reduced data for the lattice thermal conductivity are plotted in Figs. 4 and 5. The data span the temperature range 1.7–150 K except for HgTe 2-2, for which data were obtained only below 81.5 K. The electronic thermal conductivity calculated from the Wiedemann-Franz law, $\kappa_E = L_0 \sigma T$ (where $L_0 = 2.44\times10^{-8}$ W Ω K^{-2}), has been subtracted from the total thermal conductivity to obtain the points shown. Below 100 K, the electronic thermal conductivity was negligible, and even for the highest conductivity sample (HgTe 2-3) it was only 4%

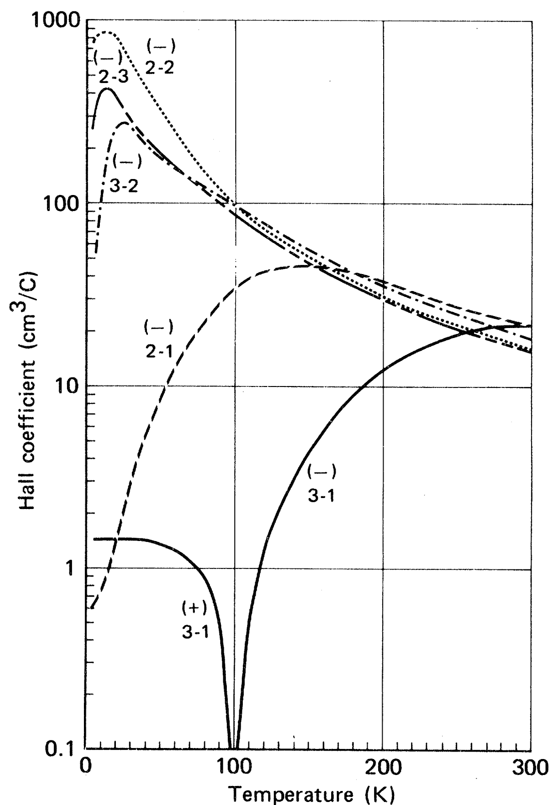

FIG. 2. Hall coefficient as function of temperature for the HgTe single-crystalline samples.

TABLE II. Net acceptor concentration ($N_A - N_D$), electrical conductivity, and Hall coefficient of HgTe crystals. The Hall coefficients for 4.2 K are extrapolated zero-field values, and those for higher temperatures are for 1.0 kG.

HgTe sample No.	$N_A - N_D$ (cm^{-3})	Electrical conductivity ($\Omega^{-1} cm^{-1}$) 4.2 K	77 K	290 K	Hall coefficient ($cm^3 C^{-1}$) 4.2 K	77 K	290 K
2-1	1.1×10^{18}	42	73	750	−27	−23	−22
2-2	3.5×10^{17}	36	270	1300	−730	−156	−17
2-3	5.0×10^{16}	17	250	1700	−260	−114	−17
3-1	4.4×10^{18}	95	110	280	1.4	0.87	−22
3-2	4.8×10^{17}	29	130	1100	−50	−120	−20

at 150 K. The Callaway theoretical model[16] was used to analyze the data. This model gives for the lattice thermal conductivity

$$\kappa = (K/2\pi^2 c)(I_1 + \beta I_2)\,, \tag{2}$$

where

$$I_1 = \int_0^{K\Theta/\hbar} \tau_c \left(\frac{\hbar\omega}{KT}\right)^2 \frac{e^{\hbar\omega/KT}}{(e^{\hbar\omega/KT}-1)^2}\,\omega^2 d\omega\,, \tag{3}$$

$$I_2 = \int_0^{K\Theta/\hbar} \frac{\tau_c}{\tau_N} \left(\frac{\hbar\omega}{KT}\right)^2 \frac{e^{\hbar\omega/KT}}{(e^{\hbar\omega/KT}-1)^2}\,\omega^2 d\omega\,, \tag{4}$$

and

$$\beta = I_2 \Big/ \int_0^{K\Theta/\hbar} \frac{1}{\tau_N}\left(1-\frac{\tau_c}{\tau_N}\right)\left(\frac{\hbar\omega}{KT}\right)^2 \frac{e^{\hbar\omega/KT}}{(e^{\hbar\omega/KT}-1)^2}\,\omega^2 d\omega\,. \tag{5}$$

In these equations, τ_N is the phonon relaxation time for normal momentum-conserving processes, and τ_c is the resultant relaxation time for all phonon-scattering processes. Also, K is the Boltzmann constant, Θ is the Debye temperature, $\hbar$ is Planck's constant divided by 2π, and $\omega = 2\pi\nu$, where ν is the phonon frequency. In terms of the phonon wave number q, $\omega = cq$.

The experimental results are consistent with the assumption that four phonon-scattering processes (in addition to normal processes) are effective in HgTe. At high temperatures, normal processes and umklapp scattering are dominant. Rayleigh scattering by point defects is the limiting mechanism at temperatures near which the thermal conductivity is a maximum. At low temperatures, the thermal conductivity is much lower than it would be if boundary scattering of phonons were the dominant process. The low-temperature thermal conductivity can be explained at least semiquantitatively by the scattering of phonons primarily by valence-band holes.

For the inverse relaxation time for normal processes, the expansion of Callaway will be used: $\tau_N^{-1} = B_2 T^3 \omega^2$. The phonon relaxation times for umklapp scattering, Rayleigh scattering, boundary scattering, and hole-phonon scattering will be denoted, respectively, by τ_U, τ_A, τ_B, and τ_p. The sum of the inverses of these relaxation times will be taken to give the inverse of τ_c, the relaxation time resulting from the combined effect of all phonon-scattering processes. That is,

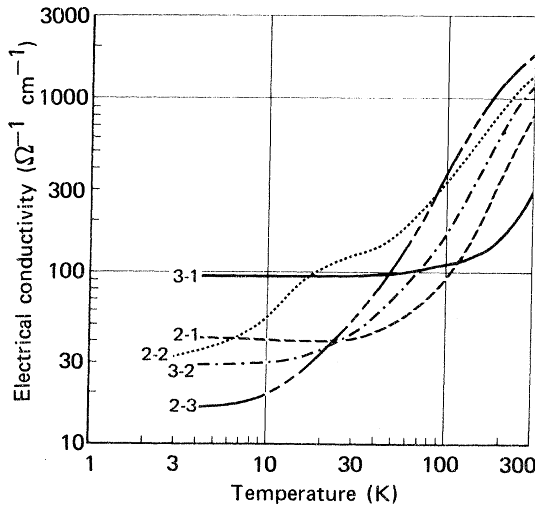

FIG. 3. Electrical conductivity as function of temperature for the HgTe single-crystalline samples.

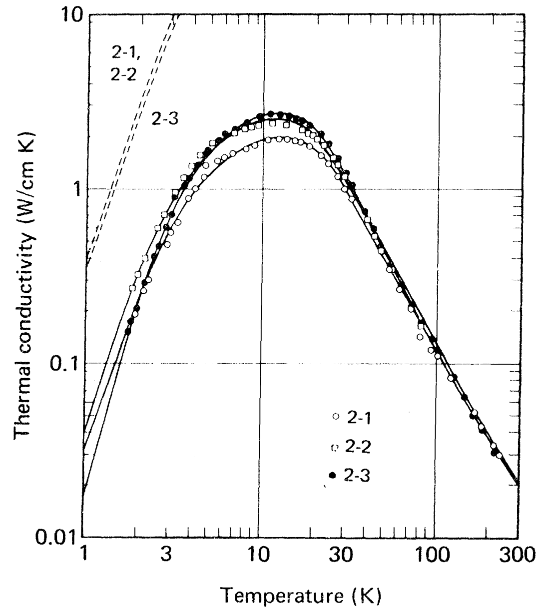

FIG. 4. Lattice thermal conductivity as function of temperature for the crystal HgTe-2 as-grown (2-1), annealed in Hg vapor at 250 °C for 100 h (2-2), and annealed in vacuum at 225 °C for 72 h (2-3). The data points shown have been corrected for electronic thermal conduction and radiation errors. The curves are the least-squares fits of the Callaway equation to the data, and the straight line is the thermal conductivity expected if diffuse scattering of phonons by crystal boundaries were to dominate.

$$\tau_c^{-1} = \tau_U^{-1} + \tau_A^{-1} + \tau_B^{-1} + \tau_p^{-1} + \tau_N^{-1} . \qquad (6)$$

For the inverse of the relaxation time for umklapp scattering, we depart from the formulation of Callaway (who used $\tau_U^{-1} = B_1 T^3 \omega^2$) and follow Slack and Galginaitis[17] who used

$$\tau_U^{-1} = B_1' T \omega^2 e^{-\Theta/aT} . \qquad (7)$$

The form of Eq. (7) gives a temperature dependence for the thermal conductivity which very closely matches that obtained experimentally. Slack and Galginaitis determined the form of Eq. (6) empirically and further derived

$$B_1' \cong \hbar \gamma^2 / M c^2 \Theta , \qquad (8)$$

where M is the average atomic mass and γ is the Grüneisen constant (here assumed to be 2.0).

For Rayleigh scattering by point defects, the inverse relaxation time is taken to be $\tau_A^{-1} = A\omega^4$. The parameter A is the sum of at least two terms: A_{isot} for the scattering caused by the natural distribution of isotopes of the elements in the compound, and A_{imp} for the scattering by point defects such as Hg and Te vacancies and interstitials.

The isotope scattering may be calculated by using the result of Klemens[18] for an isolated substitutional atom with mass difference ΔM,

$$\frac{1}{\tau_{isot}} = A_{isot}\omega^4 = \frac{a_0^3}{4\pi c^3 G}\left(\frac{\Delta M}{M}\right)^2 \omega^4 , \qquad (9)$$

where a_0^3 is the unit cell volume, G is the number of unit cells in the crystal, and M is the mass per unit cell. For each atomic species, we define the quantities $\bar{m} = \sum f_i m_i$ and $\Gamma = \sum f_i[(m_i - \bar{m})/\bar{m}]^2$, where m_i is the mass of the ith isotope and f_i is the fractional natural abundance of the isotope. Equation (9), summed over all unit cells, becomes

$$\frac{1}{\tau_{isot}} = \left[\frac{a_0^3}{4\pi c^3 G} \sum_{i=1}^{G} \left(\frac{\Delta M_i}{M}\right)^2\right] \omega^4 , \qquad (10)$$

where M is the average value for the sum of the atomic masses in a unit cell and ΔM_i is the deviation from M of the mass in the ith cell resulting from isotopic mass variations. In the case of HgTe, for which $a_0 = 6.460$ Å,[19] Eq. (10) is

$$\frac{1}{\tau_{isot}} = \frac{a_0^3}{16\pi c^3}\left(\frac{1}{\bar{m}_{Hg} + \bar{m}_{Te}}\right)^2 \times \left((\bar{m}_{Hg})^2 \Gamma_{Hg} + (\bar{m}_{Te})^2 \Gamma_{Te}\right)\omega^4$$

$$= (4.54 \times 10^{-44}\ \text{sec}^3)\omega^4 . \qquad (11)$$

Klemens[18] calculated the inverse relaxation time for substitutional atom or vacancy scattering in a monatomic crystal to be

$$1/\tau_{imp} = A_{imp}\omega^4 = (3V_0^2/\pi c^3)(\textstyle\sum_i N_i S_i^2)\omega^4 , \qquad (12)$$

where N_i is the concentration and S_i is the scattering factor of the ith type of defect, and V_0 is the atomic volume. In the case of diatomic HgTe, V_0 is the primitive unit cell volume: $V_0 = \frac{1}{4}a_0^3$. The scattering factor S_i depends in detail upon the binding forces of the defect as well as the mass change, but it usually has a value near unity. Klemens[18] calculated S_i for a number of cases of substitutional impurities or vacancies in alkali halides and obtained values ranging from 0.5 to 2.1. For HgTe,

$$1/\tau_{imp} = (6.23 \times 10^{-61}\ \text{cm}^3\,\text{sec}^3)(\textstyle\sum_i N_i S_i^2)\omega^4 . \qquad (13)$$

The inverse relaxation time for scattering of phonons by the crystal boundaries is taken to be

$$\tau_B^{-1} = c/[F(1.12\mathfrak{a}^{1/2})] , \qquad (14)$$

where $\mathfrak{a}$ is the cross-sectional area of the sample and F is related to the fraction f of phonons which are diffusely scattered at the boundaries, according to $F = (2-f)/f$. This formula for τ_B^{-1}, based upon the works of Casimir[20] and Berman, Simon, and Ziman,[21] makes no allowance for finite sample length as discussed by Berman, Foster, and Ziman.[22]

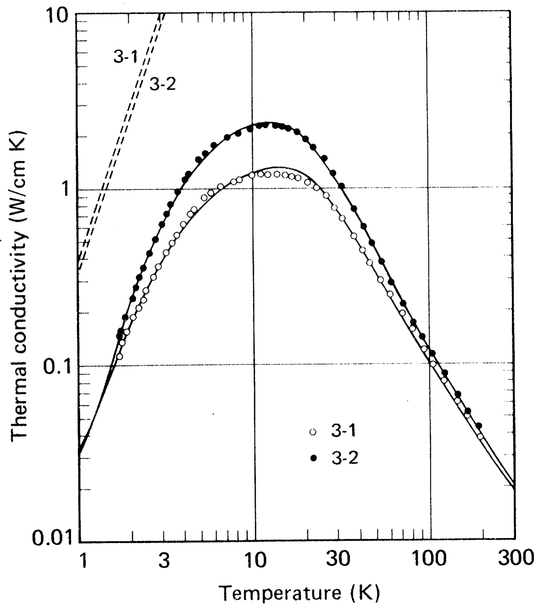

FIG. 5. Lattice thermal conductivity as function of temperature for the crystal HgTe-3 annealed at 400 °C for 1 h and then quenched (3-1) and annealed in Hg vapor at 250 °C for 100 h (3-2). The data points have been corrected for electronic thermal conduction and radiation errors. The curves are the least-squares fits of the Callaway equation to the data, and the straight lines are the thermal conductivities expected if diffuse scattering of phonons by crystal boundaries were to dominate.

TABLE III. Inverse relaxation times for various phonon-scattering mechanisms used to curve-fit thermal-conductivity data. In these expressions Θ is the Debye temperature, c is the speed of sound, $\mathcal{A}$ is the crystal cross-sectional area, and Θ_p is the hole-phonon cut-off temperature. The parameters allowed to vary in the curve-fitting are B_1', a, B_2, A, D, and Θ_p.

Umklapp processes	$\tau_u^{-1}=B_1' T\omega^2 e^{-\Theta/aT}$
Normal processes	$\tau_N^{-1}=B_2 T^3\omega^2$
Boundary scattering	$\tau_B^{-1}=c/1.12\mathcal{A}^{1/2}$
Rayleigh scattering	$\tau_A^{-1}=A\omega^4$
Hole-phonon scattering	$\tau_p^{-1}=D\omega \quad (\omega\le K\Theta_p/\hbar)$; $\tau_p^{-1}=0 \quad (\omega > K\Theta_p/\hbar)$

At low temperatures the scattering of phonons by holes in HgTe must be considered. For a simple cubic material with a spherically symmetric valence band, only longitudinal phonons should be scattered, and the inverse mean free time is[23]

$$\tau_p^{-1}=D\omega=\frac{(m_p)^2(E_{\rm def})^2\,\omega}{2\pi\rho\hbar^3\,c} \quad \text{for} \quad (\omega\le 2ck_F) \qquad (15a)$$

and

$$\tau_p^{-1}=0 \quad \text{for} \quad (\omega > 2ck_F), \qquad (15b)$$

where m_p is the hole effective mass, $E_{\rm def}$ is the lattice deformation potential, ρ is the crystal density, and k_F is the radius of the hole Fermi surface. For fcc HgTe, both transverse and longitudinal phonons should be scattered and here are assumed to have the same relaxation times. With $1/\tau_p$ contributing to the sum $1/\tau_c$, the integrals in Eqs. (3)–(5) each become the sum of two integrals; one with the limits zero and $K\Theta_p/\hbar$ and the other with the limits $K\Theta_p/\hbar$ and $K\Theta/\hbar$, where $\Theta_p = 2c\hbar k_F/K$. As a function of the hole concentrations p the hole Fermi radius is $k_F=(3\pi^2 p)^{1/3}$ if the Fermi surface is spherical, and in this case,

$$\Theta_p = 2c\hbar(3\pi^2 p)^{1/3}/K. \qquad (16)$$

IV. THERMAL CONDUCTIVITY CURVE FITTING

The thermal conductivity data were fitted by adjusting the values of B_1', B_2, a, A, D, and Θ_p in the expressions for the phonon relaxation times which are summarized in Table III. The sample dimensions and cross-sectional areas are given in Table IV. The values for the average speed of sound in HgTe, $c=1.91\times10^5$ cm/sec, and the Debye temperature, $\Theta=141$ K, were taken from Alper and Saunders.[24] Their value for Θ was calculated from the longitudinal and transverse sound velocities and should be the correct low-temperature asymptotic value. For the density ρ a value of 8.123 g/cm^3 was used which was calculated from the lattice constant $a_0=6.460$ Å.[19]

Actually, the logarithm of the thermal conductivity given by Eq. (2) was fit to the logarithms of the measured values by the method of Marquardt[25] for the least-squares estimation of nonlinear parameters. If κ_i is the thermal conductivity measured for a sample at a temperature T_i, and if $\kappa(T_i)$ is the value calculated at T_i from Eq. (2), then the curve fitting was done by finding the set of relaxation-time parameters which minimized

$$\Phi=\sum_{i=1}^{r}\left[\log_{10}\kappa_i-\log_{10}\kappa(T_i)\right]^2,$$

where r is the number of data points.

The data could be fit without hole-phonon scattering (that is, with $D=0$) if the boundary-scattering parameter F were made much smaller than unity. However, F should be unity for completely diffuse scattering of phonons at the boundaries and should be larger than unity if part of the phonons are specularly reflected. Not only were the required values of F, as small as 0.01, physically unreasonable, but data obtained for samples of different cross-sectional areas showed that the low-temperature thermal conductivity of p-type HgTe was not measurably dependent upon sample size. Only for very small samples with cross-sectional areas of about 0.01 mm^2 should boundary scattering dominate scattering by holes. Boundary scattering was, nevertheless, included in the curve fitting with F arbitrarily taken to be unity.

Because the parameters B_1', B_2, and a for the umklapp and normal processes were not expected to vary for the different samples, the data for all of the samples were fit simultaneously with only the parameters A, D, and Θ_p allowed to vary from sample to sample. The values thus found for the parameters giving the least-squares fit are compiled in Table V. If we take $[\Phi_{\rm min}/(r-s)]^{1/2}$, where s is the number of adjustable parameters, to be the standard error S_0, then for this fit with 217 data points and 18 adjustable parameters, the standard error was 0.0239. The plus and minus increments in Table V are those for which the variance ratio, $(\Phi-\Phi_{\rm min})/sS_0^2$, has the value 2.05;

TABLE IV. Dimensions and cross-sectional areas of the HgTe thermal-conductivity samples.

HgTe sample No.	Width (cm)	Thickness (cm)	Cross-sectional area (cm^2)
2-1	0.313	0.314	0.0983
2-2	0.313	0.314	0.0983
2-3	0.273	0.280	0.0765
3-1	0.315	0.316	0.0996
3-2	0.260	0.274	0.0713

TABLE V. Phonon-scattering parameters determined by curve fitting the thermal conductivity of all HgTe samples simultaneously. The parameters B_1', B_2, and a were required to be the same for all samples. and the least-squares fit was obtained with $B_1' = (9.37 \pm 0.66) \times 10^{-18}$ sec K^{-1}, $B_2 = (2.89 \pm 0.44) \times 10^{-22}$ sec K^{-3}, and $a = 1.30 \pm 0.06$. See Table III for summary of inverse relaxation time expressions containing these parameters. The hole density $p(\Theta_p)$ is derived from $p = (K\Theta_p/2c\hbar)^3/3\pi^2$. Probability is 99.0%[a] that the true value of a parameter is within the given plus and minus increments.

HgTe sample No.	$10^{44} A$ (sec^3)	$10^5 D$	Θ_p (K)	$10^{-17} p(\Theta_p)$ (cm^{-3})
2-1	93.0 ± 8.6	1.35 (+0.62, −0.36)	9.02 ± 0.40	10.0 ± 1.4
2-2	74.9 ± 7.4	1.12 (+1.20, −0.43)	8.22 ± 0.44	7.5 ± 1.2
2-3	56.8 ± 5.0	3.02 (+5.38, −1.28)	9.21 ± 0.30	10.7 ± 1.1
3-1	160 ± 14	1.24 (+0.32, −0.23)	9.29 ± 0.50	10.9 ± 2.7
3-2	67.7 ± 6.2	1.38 (+0.52, −0.33)	9.71 ± 0.38	12.4 ± 1.4

[a]Probability is based upon Snedecor's F (variance ratio) distribution tables in *Handbook of Mathematical Functions*, Natl. Bur. Std. (U.S.) Appl. Math. Series 55, edited by M. Abramowitz and I. A. Stegun (U.S. GPO, Washington, D.C., 1964), pp. 986–989.

this value for the variance ratio implies a probability of 0.990 that the true values of the parameters lie within the given limits. Because of the high degree of correlation of the parameters D and Θ_p, the variation of these parameters from sample to sample was statistically not significant. A second fit was made, for which D was required to be the same for all samples and only A and Θ_p were allowed to vary from sample to sample. This second fit, the results of which are compiled in Table VI, had a slightly greater standard error of 0.0245. In Figs. 4 and 5, the curves were calculated by using the parameters from Table V.

The values of the parameters required to fit the thermal conductivity data are of the same magnitudes that usually are found for other materials. The theoretical basis for these parameters is not sufficient to insist upon agreement with experiment better than to within a factor of two. The parameter B_1' in the expression for the unklapp relaxation time, Eq. (7), is about 9×10^{-18} sec K^{-1}. The formula of Slack and Galginaitis,[17] Eq. (8), gives in the case of HgTe, $B_1' = 3.0 \times 10^{-18}$ sec K^{-1}, if the Grüneisen constant is 2.0 and if the appropriate sound velocity is 1.91×10^5 cm/sec. This agreement must stand as satisfactory inasmuch as Eq. (8) is an approximation, the Grüneisen constant for HgTe is not known, and the appropriate values that should be used for the Debye temperature and speed of sound in HgTe are not unequivocally established at temperatures for which umklapp scattering is dominant. The parameter a in the exponential term of the expression for the umklapp relaxation time, Eq. (7), should be of the order unity, and the data fitting always required a value for a near unity.

The Rayleigh scattering parameter A is given to within ±10% by the empirical formula

$$A = (6.1 \times 10^{-43} + 2.3 \times 10^{-61} p) \text{ sec}^3, \qquad (17)$$

where p is the low-temperature hole concentration in cm^{-3}. The concentration-dependent term is given by Eq. (13) if p is substituted for N_i and if $S_i = 0.60$. The constant term in Eq. (17) is larger than A_{isot} [Eq. (9)] by a factor of 13, and such a large discrepancy forces one to conclude that other scattering processes are operative. A simple hypothesis is that each sample had a concentration of neutral defects, $N = 9 \times 10^{17}$ cm^{-3}, with a scattering factor of unity. Then Eq. (13) yields a neutral defect contribution to A of 5.7×10^{-43} sec^3, which added to the calculated value of A_{isot} gives the constant term in Eq. (17).

The best collective value for D, 1.40×10^{-5} as given in Table VI, implies that $E_{def} = 0.52$ eV if the hole effective mass is 0.53m. The Θ_p values, between 8.1 and 9.8 K, imply hole concentrations between 7×10^{17} and 1.3×10^{18} cm^{-3}, whereas the analysis of the electrical data gave a range of hole concentrations from 5.0×10^{16} to 4.4×10^{18} cm^{-3}.

The value for D of 1.4×10^{-5}, which gives $1/\tau_p = 1.4 \times 10^{-5} \omega$ sec^{-1} $= 2.7 q$ sec^{-1}, is of the magnitude predicted by theory. The expression for D, Eq. (15a), should be multiplied by some factor less than unity because the polarization of the longitudinal acoustic waves is not parallel with the wave vector

TABLE VI. Phonon-scattering parameters determined by curve fitting the thermal-conductivity data of all HgTe samples simultaneously. In addition to B_1', B_2, and a, the hole-phonon-scattering parameter D was required to be the same for all samples. The least-squares fit was obtained with $B_1' = (9.30 \pm 0.63) \times 10^{-18}$ sec K^{-1}, $B_2 = (3.00 \pm 0.41) \times 10^{-22}$ sec K^{-3}, $a = 1.30 \pm 0.05$, and $D = (1.40 \pm 0.21) \times 10^{-5}$. See Table III for summary of inverse relaxation time expressions containing these parameters. The hole density $p(\Theta_p)$ is derived from $p = (K\Theta_p/2c\hbar)^3/3\pi^2$. Probability is 99.0% that the true value of a parameter is within the given plus and minus limits.

HgTe sample No.	$10^{44}A$ (sec^3)	Θ_p (K)	$10^{-17} p(\Theta_p)$ (cm^{-3})
2-1	92.0 ± 7.7	9.01 ± 0.38	9.9 ± 1.3
2-2	73.7 ± 6.5	8.12 ± 0.39	7.3 ± 1.0
2-3	55.0 ± 4.6	9.82 ± 0.35	12.9 ± 1.4
3-1	159 ± 13	9.07 ± 0.41	10.1 ± 1.5
3-2	66.9 ± 5.5	9.73 ± 0.35	12.5 ± 1.4

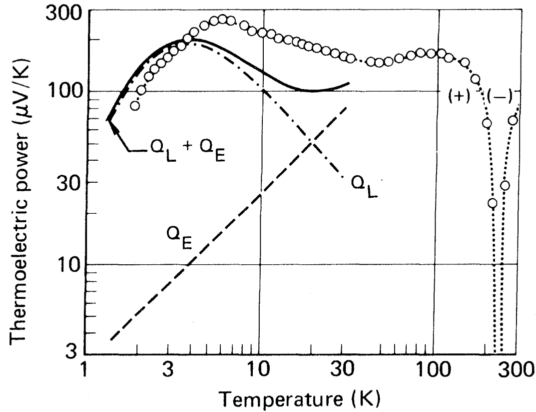

FIG. 6. Thermoelectric power as function of temperature for HgTe 3-1. The dash-dot curve is the phonon-drag contribution calculated from thermal conductivity parameters, and the dash curve is the calculated electronic contribution. The solid curve is the calculated total thermoelectric power.

as is assumed in the derivation of $1/\tau_p$. Furthermore, D should be different for longitudinal and transverse phonons. If Eq. (15a) were to give an effective average value for D, it would need to be multiplied by some factor less than unity—perhaps as small as one-third. The deformation potential is, therefore, substantially underestimated if the experimental value for D is substituted into Eq. (15a) as it stands. Compensating to some degree for this, however, is the effect of the probable reentrant shape of the hole Fermi surface, as will be pointed out in Sec. VI.

The result that the cutoff temperature Θ_p is between 8.1 and 9.8 K for all samples implies two things. First, relatively small-wavelength phonons can be scattered even for quite low hole concentrations. Second, the minimum wavelength of phonons which interact with holes is not significantly dependent upon the hole concentration. Neither of these implications can be valid for a simple parabolic valence band. On the contrary, the valence band cannot have its maximum at the center of the Brillouin zone, and its shape must be such that the maximum wave number for holes changes relatively little as the hole concentration changes.

The preceding discussion of the hole-phonon-scattering parameters must be tempered by pointing out that the thermal-conductivity data reported here do not extend to temperatures sufficiently low to yield unequivocal values for Θ_p and D. Only at temperatures lower than 1 K would the major contribution to the thermal conductivity be by the long-wavelength phonons which can interact with holes (those for which $q < K\Theta_p/\hbar c$). At 1.7 K, the lowest temperature for data reported here, only about one-third of the heat is transported by long-wavelength phonons, and at 4.2 K, only about one-tenth. To satisfactorily establish the precise nature and hole-concentration-dependence of the hole-phonon scattering, data for temperatures between 0.1 and 1 K would be required. Nevertheless, the results here demonstrate that hole-phonon scattering is important at low temperatures, although they do not exclude the possibility that other scattering mechanisms also may contribute.

To complement the results presented here, data are required for HgTe samples which are unequivocally n-type; for such samples the scattering of phonons by electrons should be small because of the low electron effective mass, and boundary scattering of phonons should prevail at low temperatures. We were not able to prepare suitable n-type HgTe to verify this prediction.

V. THERMOELECTRIC POWER

In Figs. 6 and 7, the thermoelectric power Q is shown as a function of temperature for HgTe samples 2-3 and 3-1, respectively. The peaks at low temperatures are caused by phonon drag, which may be related to the hole-phonon scattering evident in the thermal conductivity.

The total thermoelectric power is the sum of an electronic part Q_E and a phonon drag part Q_L. For a two-carrier system the electronic part is

$$Q_E = (\sigma_n Q_n + \sigma_p Q_p) / (\sigma_n + \sigma_p) , \tag{18}$$

where σ is the electrical conductivity and the subscripts n and p refer to the electron and hole contributions, respectively. This relation may be rewritten as

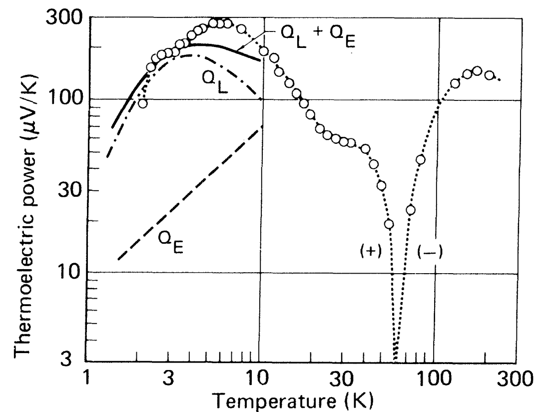

FIG. 7. Thermoelectric power as function of temperature for HgTe 3-1. The dash-dot curve is the phonon-drag contribution calculated from thermal-conductivity parameters, and the dash curve is the calculated electronic contribution. The solid curve is the calculated total thermoelectric power.

$$Q_E = [Q_p + (n/p)\, bQ_n] / [1 + (n/p)\, b] , \tag{19}$$

where n is the conduction-electron density and b is the ratio of the electron mobility to the hole mobility. For either electrons or holes, the electronic part of the thermoelectric power is given[26] by

$$Q_i = \frac{\pi^2 K^2 T}{3e} \left(\frac{\partial \ln \Lambda_i}{\partial E_i} + \frac{\partial \ln A_i^F}{\partial E_i} \right)_{E_i = \zeta_i} , \tag{20}$$

where i stands for n or p, E is the energy, ζ is the Fermi energy, A^F is the Fermi-surface area, e is the magnitude of the electron charge, and Λ is the carrier mean free path. For spherical Fermi surfaces $\Lambda_i = (2E_i/m_i)^{1/2}\tau_i$ and $A_i^F = 8\pi m_i E_i/\hbar^2$. For low temperatures τ_i is determined by the scattering of charge carriers by ionized impurities and is, according to Conwell and Weisskopf,[27]

$$\tau_i = \frac{(\frac{1}{2} m_i)^{1/2} (2a_I/\pi)(2/E_I)^2 E_i^{3/2}}{\ln[1 + (2E_i/E_I)^2]} , \tag{21}$$

where $a_I = (N_A + N_D)^{-1/3}$ (N_A is the ionized acceptor density, and N_D is the ionized donor density) and $E_I = 2e^2/\epsilon a_I$ (ϵ is the dielectric constant). With this formula for τ_i, Eq. (20) becomes

$$Q_i = \frac{\pi^2 K^2 T}{3e\zeta_i} \left[3 - \frac{2(2\zeta_i/E_I)^2}{[1 + (2\zeta_i/E_I)^2] \ln[1 + (2\zeta_i/E_I)^2]} \right] . \tag{22}$$

To evaluate this expression for Q_i, N_D was neglected and values for N_A were taken from Table I. Equations (32)–(34) of the Appendix were used to calculate n, p, and ζ_i as functions of temperature. For the value of the ratio b, $(m_p/m_n)^{3/2}$ was used in Eq. (19). For samples HgTe 2-3 and HgTe 3-1, the electron contribution to Q_E is small in comparison with the hole contribution for temperatures below 30 K, and neglect of the electrons causes errors certainly no larger than other errors inherent in the formulation.

To relate the phonon-drag part of the total thermoelectric power to the lattice thermal conductivity, the following crude analysis was made. Under the influence of a positive temperature gradient $\partial T/\partial x$, the long-wavelength phonons which can interact with holes gain a net momentum P_L in the $-x$ direction. A fraction of this momentum is transferred to the holes causing a hole concentration gradient and consequent negative voltage gradient $\partial V/\partial x$. The rate at which momentum is transferred to the holes by the phonons, $\partial P_L/\partial t = -P_L/\langle \tau_p \rangle$, added to the rate at which hole momentum, P_p, is induced in the opposite direction by the voltage gradient, $\partial P_p/\partial t = -pe(\partial V/\partial x)$, must be zero for a steady state. Now, $P_L = j_L/c^2$, where j_L is the total heat current carried by the long-wavelength phonons, and $j_L = -\kappa_L(\partial T/\partial x)$, where κ_L is the thermal conductivity attributable to long-wavelength phonons. Thus, $[\kappa_L/(c^2\langle\tau_p\rangle)](\partial T/\partial x) = pe(\partial V/\partial x)$, or

$$Q_L = \frac{(\partial V/\partial x)}{(\partial T/\partial x)} = \frac{\kappa_L}{pec^2 \langle \tau_p \rangle} . \tag{23}$$

This is substantially the result derived by Ziman[28] from a variational calculation. If Eq. (15a) is used for τ_p, the main deficiency of Eq. (23) is that the effect upon the relaxation time by the perturbation of the hole distribution function is ignored. If the calculation of the phonon drag were done in a completely self-consistent manner, the saturation effect[29] caused by the simultaneous displacements of the hole and phonon distributions would reduce the magnitude of the calculated thermoelectric power. The average of τ_p over the long-wavelength-phonon distribution is

$$\langle \tau_p \rangle = \frac{\hbar}{DKT} \frac{J_3(\Theta_p/T)}{J_4(\Theta_p/T)} , \tag{24}$$

where D is given by Eq. (15a), Θ_p by Eq. (16), and

$$J_n(\Theta_p/T) = \int_0^{\Theta_p/T} \frac{Z^n e^z dz}{(e^z - 1)^2} . \tag{25}$$

The values for the parameters from the second group fit were used in Eqs. (3)–(5), but with the limits of integration $K\Theta_p/\hbar$ rather than $K\Theta/\hbar$, to calculate κ_L and in Eq. (24) to calculate $\langle\tau_p\rangle$ for HgTe 2-3 and HgTe 3-1. Finally, $Q = Q_L + Q_E$ was calculated for these two samples from Eqs. (22) and (23). The results are plotted in Figs. 6 and 7. The agreement between the calculated and measured values is good in view of the crudity of the calculations, and we believe that this strongly supports the hypothesis that hole-phonon scattering is the dominant mechanism limiting the low-temperature thermal conductivity in p-type HgTe.

VI. DISCUSSION

The item of main interest for discussion is the depression of the thermal conductivity at low temperatures which we attempt to account for by hole-phonon scattering. Boundary scattering can be eliminated as a limiting factor. Not only is the calculated boundary scattering much too small to account for the observations, but the low-temperature thermal conductivity was not measurably dependent upon the sizes of the samples. Although the data do not extend to sufficiently low temperatures to provide a test for the presence of a resonance scattering process, the low-temperature data reported here can be fit very well by any of the resonance formulas generally employed. We disregard resonance scattering because the calculated hole-phonon interaction is the correct magnitude to fit the thermal conductivity data, and these data in turn predict reasonably well the phonon-drag contribution to the thermoelectric power.

To fit the low-temperature thermal-conductivity data with a hole-phonon relaxation time given by

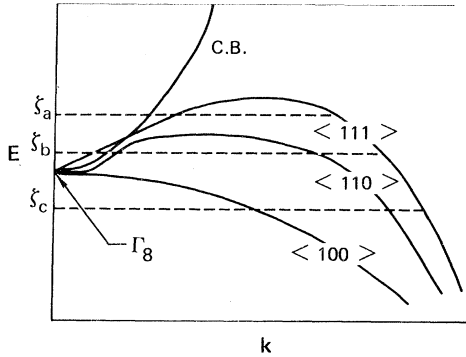

FIG. 8. Qualitative depiction of overlap of conduction band in HgTe with valence band in various directions. The positions ζ_a, ζ_b, and ζ_c for the Fermi energy give the hole Fermi surfaces shown in Figs. 9(a)–9(c), respectively.

Eq. (15a), it was necessary that Θ_p be nearly the same for all samples even though the electrical data imply that the hole concentrations of the different samples vary by two orders of magnitude. This inconsistency is a result of the assumption of a parabolic valence band, upon which Eq. (15a) is based, whereas the actual valence band structure in HgTe is not simple.

From symmetry considerations the valence band must overlap the conduction band for $\vec{k}$ in the $\langle 111\rangle$ and $\langle 100\rangle$ directions as indicated in Fig. 8.[30] An unsolved problem is the magnitude of the energy overlap, although on the basis of calculations which have been performed, the overlap must be quite small[31] and probably much smaller even than 0.001 eV. If for sufficiently small hole concentrations, the Fermi energy is at the level ζ_a shown in Fig. 8, then the hole Fermi surface will be eight ellipsoids oriented along the $\langle 111\rangle$ directions as shown in Fig. 9(a). As more holes are added, the Fermi level will drop to ζ_b in Fig. 8, and the ellipsoidal surfaces will be joined with one another to form the re-entrant Fermi surface, with many empty states at small k values, as shown in Fig. 9(b). Finally, with the addition of many holes, the Fermi energy will fall below the Γ_8 energy to a level ζ_c as indicated in Fig. 8, and the highly warped Fermi surface shown in Fig. 9(c) will result. For very large hole densities, the Fermi surface will be relatively more smooth and the parabolic valence band will be better as an approximation. The magnitudes of the valence band overlaps do not qualitatively change this picture of the evolution of the hole Fermi surface, but of course the rate of evolution as the hole density is increased does depend upon the amounts of overlap.

The essential features of the hole Fermi surface that affect the dependence of hole-phonon scattering upon hole concentration are (1) even for very small hole concentrations the maximum dimension of the Fermi surface, and hence Θ_p, is relatively large compared with the parabolic band model; (2) the maximum dimension of the Fermi surface increases slowly as holes are added; (3) the re-entrant sur-

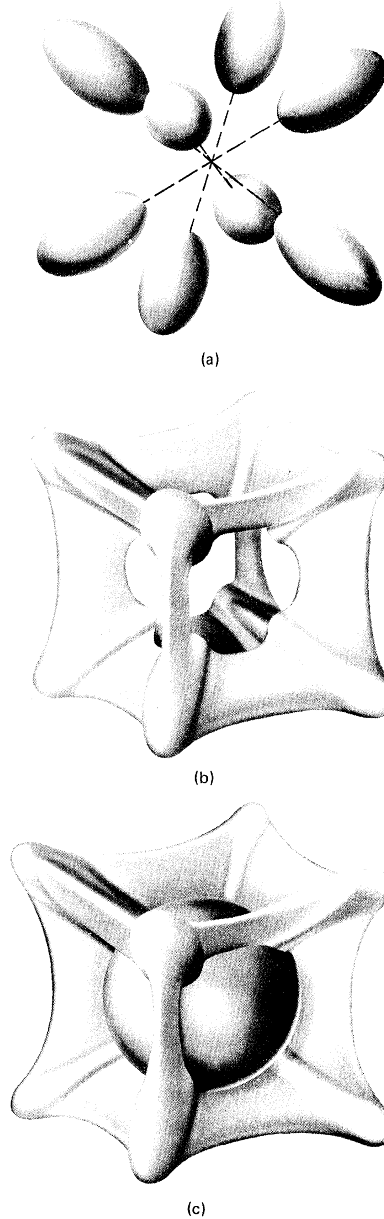

FIG. 9. Evolution of the hole Fermi surface of HgTe as the hole concentration is increased: (a) Fermi energy just below maximum valence-band energy in $\langle 111\rangle$ direction; (b) Fermi energy just below maximum valence-band energy in $\langle 110\rangle$ direction; (c) Fermi energy below bottom of conduction band.

face makes possible a larger number of momentum- and energy-conserving hole-phonon interactions than would a Fermi surface everywhere convex. The inverse of the relaxation time of the phonon distribution function when hole-phonon scattering dominates is[32]

$$\frac{1}{\tau_p}=\frac{(E_{\text{def}})^2 q}{4\pi^2\rho c}\int dk_x\int dk_y\int dk_z \times [f^0_{\vec{k}}(1-f^0_{\vec{k}+\vec{q}})\,\Theta(\Delta E)] , \quad (26)$$

where f^0 is the Fermi-Dirac distribution function, $\Theta(E)=[\sin(Et/\hbar)]/\pi E$, and $\Delta E=E_{\vec{k}}+\hbar\omega_q-E_{\vec{k}+\vec{q}}$. If $E=\hbar^2k^2/2m_p$, Eq. (26) reduces to

$$\frac{1}{\tau_p}=\frac{(E_{\text{def}})^2 m_p}{2\pi\hbar^2\rho c}\int_{k_0}^{\infty} f^0_{\vec{k}}(1-f^0_{\vec{k}+\vec{q}})\,k\,dk , \quad (27)$$

where $k_0=|(q/2)-m_pc/\hbar|$ and where the integration is over only the modulus of k. For strong degeneracy, provided $k_0<k_F$, the integral has the value $m_p\omega_q/\hbar$, and Eq. (15a) follows. If q is larger than $2k_F$, the integral in Eq. (27) is zero and Eq. (15b) is the result. For a more complex dependence of E upon $\vec{k}$, such as in the case of the HgTe valence band, some qualitative aspects of Eq. (27) can be readily ascertained. The product $f^0_{\vec{k}}(1-f^0_{\vec{k}+\vec{q}})$ restricts the integration to those $\vec{k}$ vectors which terminate on or very near the Fermi surface. The function $\Theta(\Delta E)$ has an appreciable magnitude only for $\Delta E=0$, or $E_{\vec{k}}=E_{\vec{k}+\vec{q}}-\hbar\omega_q$. For a Fermi surface which is everywhere convex, this energy conservation requirement defines a surface in $\vec{k}$ space, and only $\vec{k}$ vectors which terminate on this surface contribute to the integral in Eq. (26). However, for a reentrant Fermi surface such as in Figs. 9(a) and 9(b), the energy conservation requirement defines two or three surfaces for a range of $\vec{q}$ vectors, and the integral correspondingly should be two or three times larger. Thus, in the case of HgTe, not only is it reasonable to expect Θ_p to vary only slowly with p, but the parameter D obtained by curve fitting should be appreciably larger than would be predicted on the basis of a parabolic valence band. This compensates to some degree for the error of the assumption in Sec. IV that longitudinal and transverse phonons are scattered equally by holes.

Yet another factor may be of importance in considering the magnitude of hole-phonon scattering in HgTe. On a Fermi surface such as depicted in Fig. 9(c), there will be many nonequivalent points for which the corresponding hole group velocities will be either parallel or antiparallel. For $\vec{q}$ vectors joining such points, the phonon dispersion curve may have a larger than average slope[33]; that is, the phonon group velocity will be increased. This is the so-called Kohn anomaly.[34] The phonons with such wave vectors will interact with holes considerably more strongly than the other phonons, and the net effect may be not unlike a resonance scattering for phonon wave numbers a few times smaller than the maximum value of $2k_F$.

The thermal-conductivity curve fitting yields Θ_p ~9 K. This temperature corresponds to a value for q of 6.0×10^6 cm^{-1}. If the k value at the point of maximum overlap is about one-half the maximum k value on the Fermi surface, and if $q_{\max}=2k_{\max}$, then one deduces that the maximum overlap occurs for $k\sim1.5\times10^6$ cm^{-1}. If the phonon dispersion curves for HgTe were well known, one might contemplate the seemingly unlikely prospect of using thermal conductivity measurements to determine the valence band structure.

ACKNOWLEDGMENTS

We are grateful to E. C. Paxhia who did the computer programming for the least-squares determination of nonlinear parameters. We appreciate the aid and the many helpful discussions with Dr. A. Lehoczky and Dr. J. G. Broerman. We are particularly indebted to Dr. D. P. Ames for his helpful technical consultation, encouragement, and support of this research.

APPENDIX

The method used to calculate the electron and hole concentrations as functions of temperature will be outlined here. Because of the slight overlap of the conduction and valence bands, and because of the large density of states in the valence band, the electron concentration in moderately p-type HgTe will be appreciable even at very low temperatures. Since the electrons are much more mobile than the holes, their effect upon the electrical properties cannot be ignored, and this of course makes it difficult to calculate either of the charge carrier concentrations.

For a two carrier system, the electrical conductivity and Hall coefficient are

$$\sigma=e(n\mu_n+p\mu_p) , \quad (28)$$

and

$$R_H=-e(n\mu_n^2-p\mu_p^2)/\sigma^2 . \quad (29)$$

In these equations, n and p are the conduction electron and hole densities and μ_n and μ_p are the electron and hole mobilities. Knowledge of σ and R_H is insufficient to determine the four unknowns n, p, μ_n, and μ_p. There is no justification for assuming that the mobility ratio $b=\mu_n/\mu_p$ is independent of temperature or that this ratio at a given temperature is the same for all samples. The electron mobility is, however, much larger than the hole mobility at all temperatures: Near room temperature, where the electron and hole concentrations are comparable in magnitude, we therefore assume

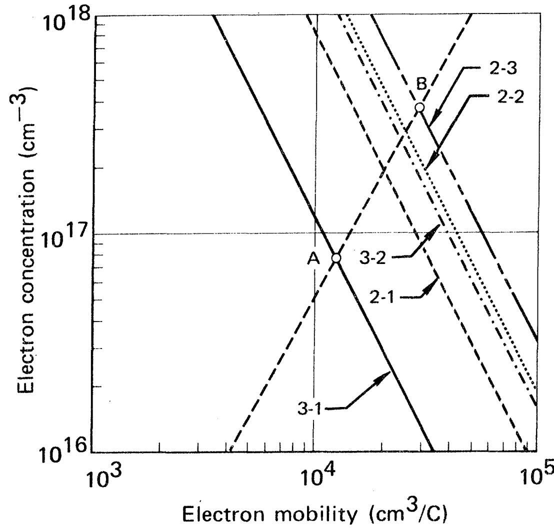

FIG. 10. Electron concentration as function of mobility at 290 K. The lines for the various HgTe samples are based upon the measured R_H and σ values substituted into the relation $n=(-R_H\sigma/e)/\mu_n^2$. The actual value of n for each sample is determined from the intersection of its line with the dashed line connecting points A and B, which is the empirically determined dependence of n upon μ_n at 290 K.

that $n\mu_n^2 \gg p\mu_p^2$. With this assumption, the combination of Eqs. (28) and (29) gives

$$n=-eR_H\sigma^2/\mu_n^2. \tag{30}$$

Equation (30) can be used to calculate n near room temperature if μ_n is known, or μ_n if n is known, from the measured values of R_H and σ. On a log-log plot, the possible solutions for n as a function of μ_n must lie on a straight line with a slope of −2. Such plots for the five HgTe samples, derived from R_H and σ values at 290 K, are shown in Fig. 10. The point A in Fig. 10 for HgTe 2-3 was established by assuming that for this sample at 290 K the Hall coefficient was very nearly $R_H=-1/ne$, which gives $n=3.7\times10^{17}$ electrons/cm^3. The net acceptor concentration for HgTe 3-1 was assumed to be identical with the low-temperature hole concentration which, for this sample, is $p=1/R_He=4.4\times10^{18}$ holes/cm^3. Using a method outlined in the following paragraph and the above value for the net accepter concentration, the value of n at 290 K was calculated to be 7.5×10^{16} electrons/cm^3, and this value determined the point B in Fig. 10. It next was assumed that at 290 K the electron mobility varied as some power of the electron concentration[35]; thus, in Fig. 10, the solution for n and μ_n for each sample should be the intersection of its log n-log μ_n plot with the straight line through points A and B. In this manner a value for n at 290 K for each sample was determined, and from this value the net acceptor concentration for the sample was calculated by the method described next.

Both n and p, as functions of temperature, were calculated for the simple band structure shown in Fig. 11. The valence band of the simplified model is assumed to be parabolic and to have its maximum at the zone center at an energy A relative to the minimum energy of the conduction band. Except at very low temperatures, this model is adequate because the effects of the detailed nature of the overlap and the shape of the valence band are obscured as the temperature is increased. The conduction band is assumed to be given by the Kane formula,[36]

$$E=\hbar^2k^2/2m-\tfrac{1}{2}E_G+(E_G^2+\tfrac{8}{3}P^2k^2)^{1/2}, \tag{31}$$

where m is the free-electron mass, E_G is the $\Gamma_6-\Gamma_8$ band separation at zone center, and P is the interband momentum matrix element. If N_A and N_D are the ionized acceptor and donor concentrations, respectively, then

$$p-n=N_A-N_D, \tag{32}$$

$$p=\frac{4\pi(2m_p)^{3/2}}{\hbar^3}\int_0^\infty \frac{E^{1/2}\,dE}{e^{(E-\zeta')/KT}+1}, \tag{33}$$

and

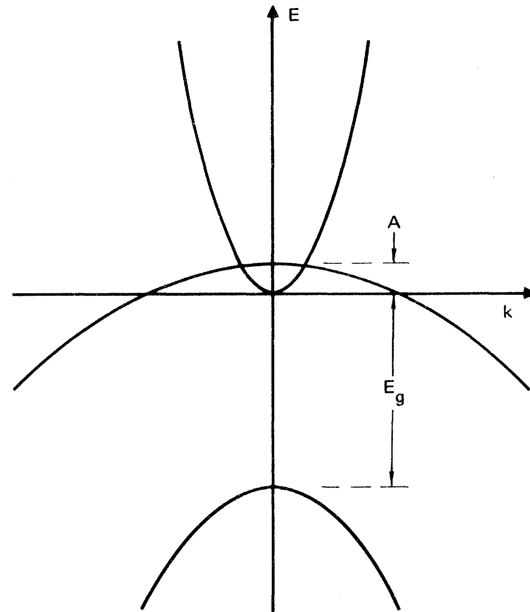

FIG. 11. Simplified band structure used for calculations of charge carrier densities in HgTe. Actually, the conduction and valence bands are degenerate at the zone center, and the overlap occurs away from the zone center in only certain directions (see Fig. 8).

$$n=\frac{4\pi(2m)^{3/2}}{\hbar^3}\int_0^\infty \frac{[E+(E_G/\mu)R]^{1/2}[(R+\mu)/(R+1)]\,dE}{e^{(E-\zeta')/KT}+1}, \quad (34)$$

where $\zeta'=A-\zeta$, $\mu=(3\hbar^2E_G)/(4P^2m)$, and $R=[1+(4E\mu/E_G)(1-\mu)]^{1/2}-1$. We assume N_A-N_D to be independent of temperature and use the following parameter values: $m_p=0.53m$,[37] $E_G=0.30[1-0.00167(T-4.2)]$ eV,[38] $P=3.8\times10^{-8}$ eV cm,[39,40] and $A=0.001$ eV.[41] For each sample the value for n at 290 K was read from Fig. 10 and substituted into Eqs. (32)–(34), which then were solved simultaneously to yield N_A-N_D. The results are given in Table II.

To this point all of the samples have been considered to be p-type ($p>n$), and on this basis all of the electrical data can be analyzed in a self-consistent manner. However, the behavior of HgTe 2-2 is qualitatively similar to that of n-type samples as reported by Ivanov-Omskii *et al.*[42] It is not possible to self-consistently analyze the electrical data for HgTe 2-2 on the basis that it is n-type because its room-temperature Hall coefficient is significantly larger than that for intrinsic samples reported in the literature as well as larger than that calculated on the basis of our assumed band model. The actual character of HgTe 2-2 cannot be resolved beyond the statement that it must be highly compensated and have nearly intrinsic concentrations of electrons and holes at temperatures above 10 K.

*Research was conducted under the McDonnell Douglas Independent Research and Development Program.

[1]S. Groves and W. Paul, Phys. Rev. Letters 11, 194 (1963).

[2]S. Groves and W. Paul, in *Proceedings of the Seventh International Conference on the Physics of Semiconductors* (Dunod, Paris, 1964), p. 41.

[3]T. C. Harman, W. H. Kleiner, A. J. Strauss, G. B. Wright, J. G. Mavroides, J. M. Honig, and D. H. Dickey, Solid State Commun. 2, 305 (1964). For discussions of the evidence for the band structure of HgTe as well as reviews of the general properties of this compound, see T. C. Harman, in *Physics and Chemistry of II-VI Compounds*, edited by M. Aven and J. S. Prener (North-Holland, Amsterdam, 1967), Chap. 15, p. 767; T. C. Harman, in *II-VI Semiconducting Compounds*, 1967 *International Conference*, edited by D. G. Thomas (W. A. Benjamin, New York, 1967), p. 982.

[4]E. L. Stelzer, J. L. Schmit, and O. N. Tufte, IEEE Trans. Electron. Devices ED-16, 880 (1969).

[5]R. O. Carlson, Phys. Rev. 111, 476 (1958).

[6]E. E. Kolosov and P. V. Sharavskii, Fiz. Tverd. Tela 7, 2247 (1965) [Sov. Phys. Solid State 7, 1814 (1966)].

[7]W. Markert, H. Nieke, and D. Spiegler, Ann. Physik 21, 387 (1968).

[8]V. M. Muzhdaba, V. K. Ogorodnikov, S. A. Aliev, and S. S. Shalyt, Fiz. Tverd. Tela 11, 545 (1969) [Sov. Phys. Solid State 11, 442 (1969)].

[9]C. R. Whitsett and D. A. Nelson, J. Crystal Growth 6, 26 (1969).

[10]W. D. Lawson, S. Nielsen, E. H. Putley, and A. S. Young, J. Phys. Chem. Solids 9, 325 (1959).

[11]W. Giriat, Brit. J. Appl. Phys. 15, 151 (1964).

[12]For an extensive study of the solid-vapor equilibrium for the Hg-Te system and a discussion of the defects in HgTe, see A. J. Strauss and R. F. Brebrick, J. Phys. Chem. Solids 31, 2293 (1970).

[13]M. G. Holland and L. G. Rubin, Rev. Sci. Instr. 33, 923 (1962).

[14]B. L. Rhodes, C. E. Moeller, and H. J. Sauer, Cryogenics 4, 17 (1964).

[15]A. C. Anderson, W. Reese, and J. C. Wheatley, Rev. Sci. Instr. 34, 1386 (1963).

[16]J. Callaway, Phys. Rev. 113, 1046 (1959).

[17]G. A. Slack and S. Galginaitis, Phys. Rev. 133, A253 (1964).

[18]P. G. Klemens, Proc. Phys. Soc. (London) A68, 1113 (1955).

[19]W. D. Lawson, S. Nielsen, E. H. Putley, and A. S. Young, J. Phys. Chem. Solids 9, 325 (1959).

[20]H. B. G. Casimir, Physica 5, 47 (1938); 5, 320 (1938); 5, 619 (1938).

[21]R. Berman, F. E. Simon, and J. M. Ziman, Proc. Roy. Soc. (London) A220, 171 (1953).

[22]R. Berman, E. L. Foster, and J. M. Ziman, Proc. Roy. Soc. (London) A231, 130 (1955).

[23]See, for example, J. M. Ziman, *Electrons and Phonons* (Oxford U. P., London, 1963), p. 330.

[24]T. Alper and G. A. Saunders, J. Phys. Chem. Solids 28, 1637 (1967).

[25]D. W. Marquardt, J. Soc. Ind. Appl. Math. 11, 431 (1963).

[26]Reference 23, p. 397.

[27]E. Conwell and V. Weisskopf, Phys. Rev. 77, 388 (1950).

[28]Reference 23, p. 409.

[29]C. Herring, Phys. Rev. 96, 1163 (1954).

[30]S. H. Groves, in *Physics of Semimetals and Narrow Gap Semiconductors*, edited by E. L. Carter and R. E. Bates (Pergamon, New York, 1971), p. 447.

[31]S. Bloom and T. K. Bergstresser, Phys. Status Solidi 42, 191 (1970).

[32]Reference 23, pp. 329ff.

[33]P. L. Taylor, Phys. Rev. 131, 1995 (1963).

[34]W. Kohn, Phys. Rev. Letters 2, 393 (1959).

[35]Calculations of the electron mobility in the case of combined optical-phonon and ionized-impurity scattering confirmed a power-law dependence of mobility upon electron concentration. This behavior results from the reduction in electron screening and consequent increase in ionized impurity scattering as the electron concentration decreases. Because of the critical dependence of the calculated mobility upon such quantities as the optical-phonon frequency and the dielectric constants, a theoretical determination could not be made of the appropriate power of electron density.

[36]E. O. Kane, J. Phys. Chem. Solids 1, 249 (1957).

[37]V. I. Ivanov-Omskii, B. T. Kolomiets, Yu. F. Markov, A. Sh. Mekhtiev, and K. P. Smekalova, Fiz. i Tekhn.

Poluprov. 1, 1442 (1967) [Sov. Phys. Semiconductors 1, 1203 (1967)].

[38]The temperature coefficient of E_G was assumed to be constant up to room temperature. The value 0.30 eV at 4.2 K is from C. R. Pidgeon and S. H. Groves, in *II-VI Semiconducting Compounds*, 1967 *International Conference*, edited by D. G. Thomas (W. A. Benjamin, New York, 1967), p. 1080. The value 0.15 eV at 300 K is from C. Verié, Phys. Status Solidi 17, 889 (1966).

[39]W. Giriat, Phys. Letters 24A, 515 (1967).

[40]W. Szymańska, Phys. Status Solidi 23, 69 (1967).

[41]The value for A was chosen to yield intrinsic carrier concentrations at low temperature that agree with the experimental data of Galazka [Phys. Letters 32A, 101 (1970)] and Ivanov-Omskii *et al.* (Ref. 42). Both Galazka and Schmit [J. Appl. Phys. 41, 2876 (1970)] have used sets of parameters slightly different from ours to calculate intrinsic carrier concentrations in HgTe. The parameters used here give results that agree closely with the data of Ivanov-Omskii *et al.* and are certainly adequate for the purposes of this paper; our calculation gives, for the intrinsic electron concentration, $n_i = 1.46 \times 10^{15}$ cm^{-3} at 4.2 K and $n_i = 4.01 \times 10^{17}$ cm^{-3} at 300 K. The results at all temperatures are sensitive to the value chosen for m_p; the low-temperature results are particularly sensitive to A. Nevertheless, a fit to experimental data can still be obtained even if any one of the parameters is changed appreciably provided compensating changes are made in other parameters.

[42]V. I. Ivanov-Omskii, B. T. Kolomiets, V. K. Ogorodinkov, and K. P. Smekalova, Fiz. i Tekh. Poluprov. 4, 264 (1970) [Sov. Phys. Semiconductors 4, 214 (1970)].

PHYSICAL REVIEW B VOLUME 5, NUMBER 8 15 APRIL 1972

Optical Properties of Semiconducting VO_2 Films*

Anibal Gavini† and Clarence C. Y. Kwan

Superior Electronics Inc., 2255 *Dandurand, Montreal, Quebec, Canada*

(Received 22 October 1971)

The reflectivity of a thick sputtered film of VO_2 has been measured in the energy range 0.5–11.0 eV at room temperature. The complex dielectric constant (ϵ_1, ϵ_2) and the complex index of refraction (n, k) have been obtained from the reflectivity measurements using the Kramers-Kronig relations. We have also measured the transverse electroabsorption spectrum of a thin sputtered film of VO_2 at liquid-nitrogen temperature. Comparison of the electroabsorption spectrum with theoretical predictions identifies the edge at 2.011 eV as corresponding to a direct transition at an M_0 edge. In spite of the lack of a band-structure calculation for VO_2, the singularities in ϵ_2 at 0.6, 1.04, 1.32, 1.82, 2.64, 3.6, 5.89, and 9.6 eV are assigned to specific interband transitions.

I. INTRODUCTION

Transition-metal oxides which show a phase transition from a semiconducting to a metallic state have been the subject of considerable interest.[1,2] Of all these materials VO_2 is the most interesting in terms of applications.[3,4] The transition in VO_2, which is a first-order semiconductor-to-metal transition, occurs at 68 °C. This transition is accompanied by a lattice distortion from a low-temperature monoclinic to a high-temperature tetragonal structure. The origin of this transition has been the subject of considerable controversy.[1,5–7] The electrical and optical properties of VO_2 have been studied extensively.[8–11] However, in most cases the stoichiometry, chemical purity, and freedom from defects of the measured VO_2 have not been high, at least by the standards of semiconductor technology, and this fact has produced a very large dispersion in the published data.

The electronic contribution to the optical properties of VO_2 has been studied by Verleur *et al.*[10] and by Borisov *et al.*[12] The temperature and pressure dependence of the energy gap has been measured by Ladd and Paul,[13] and photoemission measurements have been performed by Powell *et al.*[14] These measurements indicate that in the low-temperature phase VO_2 has an energy gap between 0.6 and 1.0 eV due to the crystal-field splitting of the uppermost partially filled vanadium 3*d* conduction band. Optical transitions at energies higher than 2.5 eV have been assigned to interband transitions between an oxygen 2*p* valence band and the lowest empty vanadium 3*d* conduction band.

Standard optical measurements, such as reflection and absorption, do not provide very high resolution for solids whose optical spectra show very large structureless backgrounds. Several modulation techniques have been developed in the last few years. By measuring the derivative of the optical spectrum with respect to some parameter, these techniques eliminate the background and enhance the structure to allow very precise determination of the energies of the transitions. These methods have proved to be useful in determining the energy of the interband transitions in semiconductors, in-

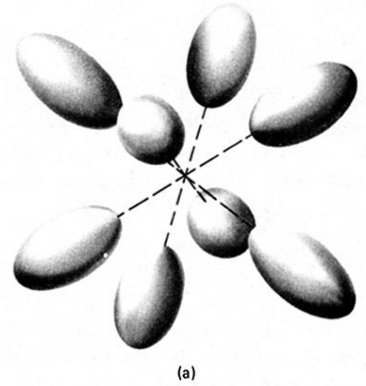

(a)

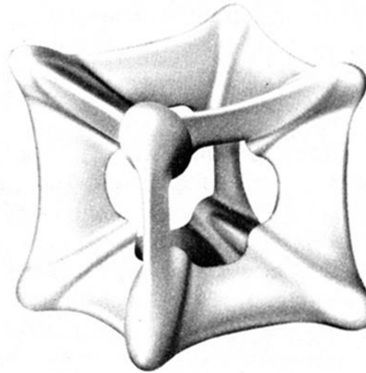

(b)

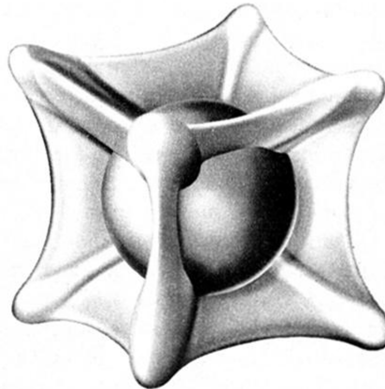

(c)

FIG. 9. Evolution of the hole Fermi surface of HgTe as the hole concentration is increased: (a) Fermi energy just below maximum valence-band energy in ⟨111⟩ direction; (b) Fermi energy just below maximum valence-band energy in ⟨110⟩ direction; (c) Fermi energy below bottom of conduction band.